JOURNAL OF MATERIALS SCIENCE **39** (2004) 2315–2325

Atomistic simulations of the solubilization of single-walled carbon nanotubes in toluene

M. GRUJICIC*, G. CAO
Department of Mechanical Engineering, Program in Materials Science and Engineering, Clemson University, Clemson, SC 29634, USA
E-mail: mica.grujicic@ces.clemson.edu

W. N. ROY
Army Research Laboratory—Processing and Properties Branch Aberdeen, Proving Ground, MD 21005-5069, USA

Solubilization of the armchair, metallic (10,10) single-walled carbon nanotubes (SWCNTs) in toluene is modeled using molecular dynamics simulations. Inter- and intra-molecular atomic interactions in the SWCNT + toluene system are represented using COMPASS (Condensed-phased Optimized Molecular Potential for Atomistic Simulation Studies), the first *ab initio* forcefield that enables an accurate and simultaneous prediction of various gas-phase and condensed-phase properties of organic and inorganic materials.

The results obtained show that due to a significant drop in the configurational entropy of toluene, the solvation Gibbs free energy for these nanotubes in toluene is small but positive suggesting that a suspension of these nanotubes in toluene is not stable and that the nanotubes would fall out of the solution. This prediction is consistent with experimental observations.

1. Introduction

Due to a unique combination of their mechanical, electrical and chemical properties, carbon nanotubes have been investigated very aggressively since their discovery in 1991 [1]. Depending on the fabrication method used, carbon nanotubes appear either predominantly as single-walled carbon nanotubes (SWCNTs) or as multi-walled carbon nanotubes (MWCNTs). SWCNTs, predominantly produced in carbon ablation and arc discharge processes, can be described as single graphene sheets rolled up into a cylinder with a quasi-one-dimensional crystal structure. Depending on their diameter and the spiral conformation (chirality), SWCNTs can be either semiconducting or metallic. Mechanical properties of SWCNTs are quite remarkable; their elastic modulus is typically above 1TPa, and they can undergo very large non-uniform (even highly localized) reversible deformations. Except for their ends and the locations of topological defects (e.g., 7-5-5-7 and Stone-Wales defects), SWCNTs are generally not very reactive.

MWCNTs are generally produced during thermal decomposition of carbon precursors. Due to a weak inter-wall bonding, MWCNTs have generally inferior mechanical properties relative to those of the SWCNTs. Their electrical properties are similar to those of the SWCNTs although they can not be easily correlated with their chirality. Chemical properties of the MWCNTs are dominated by thestructure of their outer wall and are, hence, similar to the ones of the SWCNTs.

While carbon nanotubes have been perceived as having a great potential in many critical applications (e.g., field-emission flat-panel displays [e.g., 2], novel microelectronic devices [e.g., 3], hydrogen storage devices [e.g., 4], structural reinforcement agents [e.g., 5], and chemical and electrochemical sensors [e.g., 6]), the lack of control of their purity and diameter, length and chirality distributions during fabrication is a major current obstacle to their full utilization. During fabrication of the carbon nanotubes, other materials such as carbon onions and turbostratic/amorphous graphite are also generally produced. Many techniques (e.g., oxidation) have been proposed for separation of the carbon nanotubes from the unwanted byproducts. However, a method is currently lacking for separation of the carbon nanotubes according to their diameter and/or chirality, the key geometrical and structural parameters which control electronic properties of these materials.

Recently, a new approach for carbon nanotube separation and purification has been demonstrated [7]. The method is based on non-covalent sidewall functionalization (attachment of functional groups/molecules on the outer wall) of SWCNTs and MWCNTs with π-conjugated poly(*p*-phenlyenevinylene-*co*-2, 5-dioctoxy-*m*-phenylenevinylene) (PmPV-*co*-DOct-OPV) polymer. Pristine carbon nanotubes, despite

*Author to whom all correspondence should be addressed.

Report Documentation Page

Form Approved
OMB No. 0704-0188

1. REPORT DATE	2. REPORT TYPE	3. DATES COVERED
2004		**00-00-2004 to 00-00-2004**

4. TITLE AND SUBTITLE	5a. CONTRACT NUMBER
Atomistic simulations of the solubilization of single-walled carbon nanotubes in toluene	5b. GRANT NUMBER
	5c. PROGRAM ELEMENT NUMBER
6. AUTHOR(S)	5d. PROJECT NUMBER
	5e. TASK NUMBER
	5f. WORK UNIT NUMBER
7. PERFORMING ORGANIZATION NAME(S) AND ADDRESS(ES) **Celmson University,Department of Mechanical Engineering,Clemson,SC,29634**	8. PERFORMING ORGANIZATION REPORT NUMBER
9. SPONSORING/MONITORING AGENCY NAME(S) AND ADDRESS(ES)	10. SPONSOR/MONITOR'S ACRONYM(S)
	11. SPONSOR/MONITOR'S REPORT NUMBER(S)

12. DISTRIBUTION/AVAILABILITY STATEMENT
Approved for public release; distribution unlimited

13. SUPPLEMENTARY NOTES

14. ABSTRACT

15. SUBJECT TERMS

16. SECURITY CLASSIFICATION OF:			17. LIMITATION OF ABSTRACT	18. NUMBER OF PAGES	19a. NAME OF RESPONSIBLE PERSON
a. REPORT **unclassified**	b. ABSTRACT **unclassified**	c. THIS PAGE **unclassified**	**Same as Report (SAR)**	**11**	

their hydrophobic character, are found not to be soluble in non-polar solvents such as toluene. However after functionalization with the PmPV-*co*-DOctOPV, carbon nanotubes become soluble and can be suspended in toluene. While solubilization of the carbon nanotubes through sidewall functionalization can be achieved in many different ways, it is critical that the functionalization is of a non-covalent character so that the electronic characteristics of the carbon nanotubes (governed by their sp^2 hybridization) are not altered.

In a series of papers, Blau and co-workers [7–16] carried out a detailed experimental and computational investigation of SWCNT and MWCNT solubilization in toluene through sidewall functionalization with PmPV-DOctOPV. Their atomistic simulation results showed that the backbone of the PmPV-DOctOPV molecule adopts a relatively flat helical structure which is governed by the *meta*-phenylene linkage. The van der Waals interaction between octyloxy groups, on the other hand, causes these groups to project outwards from the helical structure. This PmPV-DOctOPV conformation is shown to promote adhesion of these molecules to the nanotubes and, hence, is believed to play a critical role in the nanotubes solubilization process. While the work of Blau and co-workers [7–16] has resulted in a major improvement of our understanding of nanotubes solubilization with sidewall functionalization, two important points were not addressed in their work: (a) why hydrophobic nanotubes are not soluble in nonpolar solvents like toluene and (b) what is the role of the solvent in nanotubes solubilization by sidewall functionalization. In the present work, we investigate, using atomistic simulations, the first of the two outstanding issues, i.e., solubilization of the carbon nanotubes in toluene. While this process can be expected to be affected by the nanotubes chirality, the results obtained in the present work show that the chirality effect is minor. Hence, only the results pertaining to solubilization of the armchair metallic, (10,10) SWCNTs in toluene are presented in this paper.

The organization of the paper is as follows: A description of the computational cell, the computational method and the inter-atomic forcefield potentials used in the present work is presented in Section 2. The main results obtained in the present work are presented and discussed in Section 3, while the key conclusions resulted from the present study are summarized in Section 4.

2. Computational procedure

2.1. Computational cell

Computer simulations of the structure of pure toluene are carried out using a 2.604 nm by 2.604 nm by 2.604 nm cubic computational cell with periodic boundary conditions applied in all three principal directions. One hundred molecules are placed in the cell to obtain the average density of toluene essentially equal to its experimental counterpart (867 kg/m^3). Toluene ($C_6H_5CH_3$) is the simplest alkyl benzene, the methylbenzene, in which one of the hydrogen atoms in the benzene (C_6H_6) is replaced by a methyl group (CH_3). At room temperature, toluene is in liquid state. The geometrically optimized structure of toluene along with the atomic charges is shown in Fig. 1.

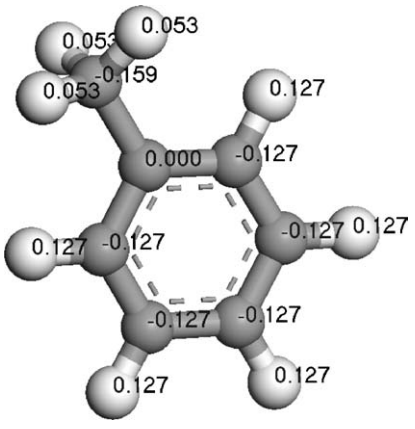

Figure 1 Geometrically optimized structure of a toluene molecule and the corresponding atomic charges.

To model the interactions between isolated (far spaced) carbon nanotubes and the toluene solvent, a 4.04 nm by 4.04 nm by 4.154 nm rectangular computational cell with periodic boundary conditions applied in all three principal directions is used. A single (10,10) SWCNT with its axis aligned in the z-direction is placed in the center of the computational cell. Thus, the SWCNT is considered as infinitely long and the end-effects associated with its hemispherical caps are neglected. The end effects are generally considered to play a minor role in the SWCNT solubilization process due to a very large (ca. 100–1000) length-to-diameter aspect ratio in the SWCNTs. The lengths of the computational cell in the x- and y-directions are sufficiently large that interactions between the SWCNTs in the adjacent cells can be neglected. 330 molecules of toluene are placed in the computational cell around the SWCNT and the size of the computational cell in the x- and y-directions adjusted until the toluene density in the regions far away from the SWCNT reached a value close to the average experimental density of toluene (867 kg/m^3).

2.2. Computational method

The (10,10) SWCNT + toluene system discussed in the previous section is modeled using classical molecular dynamics simulations in the microcanonical (NVE) ensemble. To ensure stability of the simulations and energy conservation, a constant time step of 0.2 fs is used for numerical integration of the equations of motion.

After placing the nanotube and the toluene molecules into the computational cell, the canonical (NVT) molecular simulations are first carried out for 5 ps until the system is equilibrated at a desired temperature of 300 K. Temperature control is achieved by velocity scaling which was carried out every 1 fs. Once the system is equilibrated, microcanonical (NVE) simulations are carried out for additional 5 ps and the data colleted for computation of the system properties.

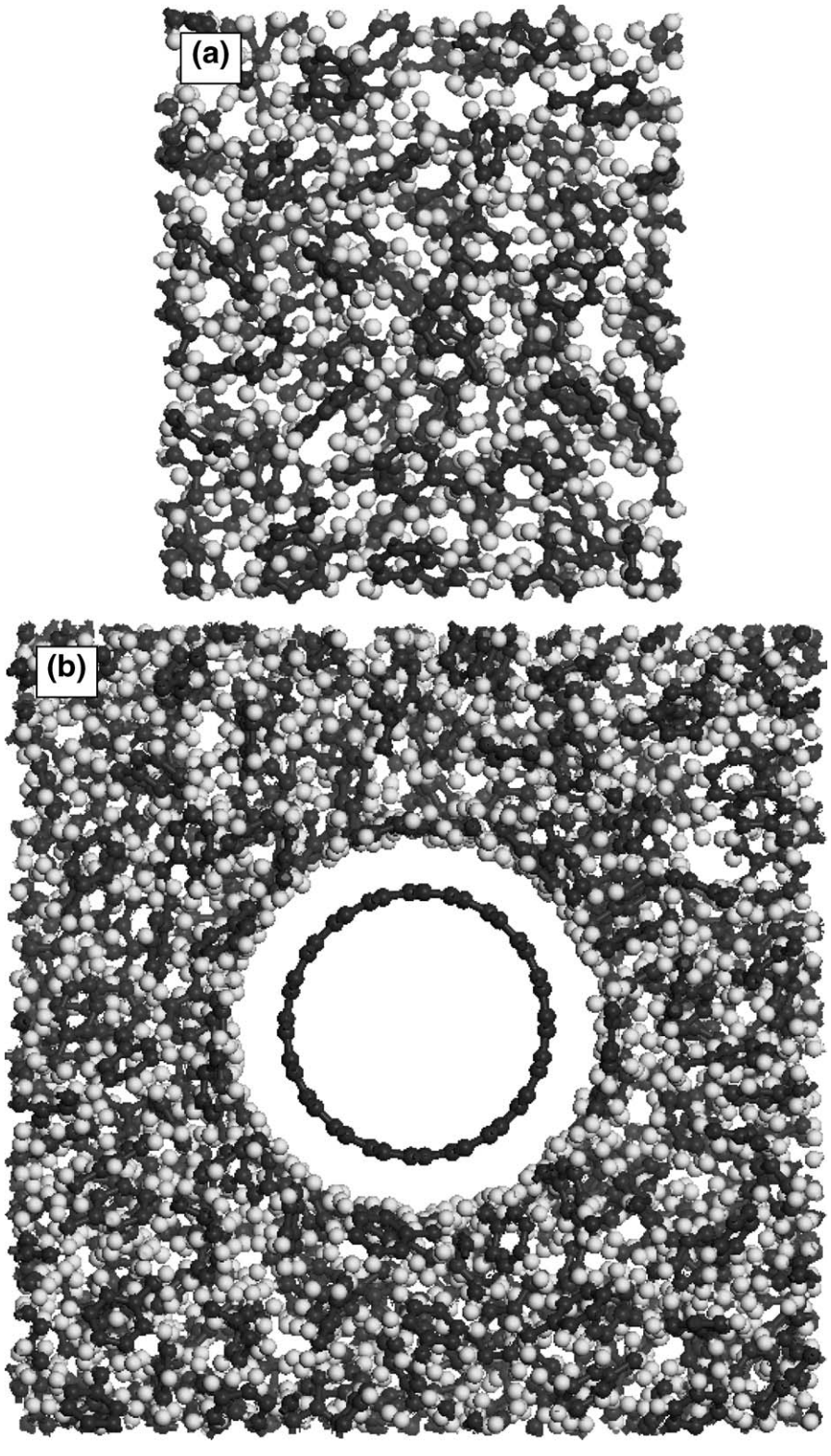

Figure 2 A snapshot of the molecular configurations for: (a) pure toluene and (b) toluene containing SWCNTs.

Snapshots of the molecular configurations in pure toluene and in toluene containing a SWCNT is shown in Fig. 2a and b, respectively.

2.3. Forcefield

While the accurate simulation of a system of interacting particles generally entails the application of quantum mechanical techniques, such techniques are computationally quite expensive and are usually feasible only in systems containing up to few hundreds of interacting particles. In addition, the main goal of simulations of the systems containing a large number of particles is generally to obtain the systems' bulk properties which are primarily controlled by the location of atomic nuclei and the knowledge of the electronic structure, provided by the quantum mechanic techniques, is not critical. Under these circumstances, a good insight into the behavior of a system can be obtained if a reasonable, physically-based approximation of the potential

(forcefield) in which atomic nuclei move is available. Such a forcefield can be used to generate a set of system configurations which are statistically consistent with a fully quantum mechanical description.

As stated above, a crucial point in the atomistic simulations of multi-particle systems is the choice of the forcefields which describe, in an approximate manner, the potential energy hypersuface on which the atomic nuclei move. In other words, the knowledge of forcefields enables determination of the potential energy of a system in a given configuration. In general, the potential energy of a system of interacting particles can be expressed as a sum of the valence (or bond), E_{valence}, crossterm, $E_{\text{crossterm}}$, and nonbond, E_{nonbond}, interaction energies as:

$$E_{\text{total}} = E_{\text{valence}} + E_{\text{crossterm}} + E_{\text{non-bond}} \quad (1)$$

The valence energy generally includes a bond stretching term, E_{bond}, a two-bond angle term, E_{angle}, a dihedral bond-torsion term, E_{torsion}, an inversion (or an out-of-plane interaction) term, E_{oop}, and a Urey-Bradlay term (involves interactions between two atoms bonded to a common atom), E_{UB}, as:

$$E_{\text{valence}} = E_{\text{bond}} + E_{\text{angle}} + E_{\text{torsion}} + E_{\text{oop}} + E_{\text{UB}} \quad (2)$$

A schematic explaining the first four types of valence atomic interactions is given in Fig. 3.

The crossterm interacting energy, $E_{\text{crossterm}}$, accounts for the effects such as bond lengths and angles changes caused by the surrounding atoms and generally includes: stretch-stretch interactions between two adjacent bonds, $E_{\text{bond-bond}}$, stretch-bend interactions between a two-bond angle and one of its bonds, $E_{\text{bond-angle}}$, bend-bend interactions between two valence angles associated with a common vertex atom, $E_{\text{angle-angle}}$, stretch-torsion interactions between a dihedral angle and one of its end bonds, $E_{\text{end\_bond-torsion}}$, stretch-torsion interactions between a dihedral angle and its middle bond, $E_{\text{middle\_bond-torsion}}$, bend-torsion interactions between a dihedral angle and one of its valence angles, $E_{\text{angle-torsion}}$, and bend-bend-torsion interactions between a dihedral angle and its two valence angles, $E_{\text{angle-angle-torsion}}$, terms, as:

$$\begin{aligned} E_{\text{crossterm}} = {} & E_{\text{bond-bond}} + E_{\text{angle-angle}} + E_{\text{bond-angle}} \\ & + E_{\text{end\_bond-torsion}} + E_{\text{middle\_bond-torsion}} \\ & + E_{\text{angle-torsion}} + E_{\text{angle-angle-torsion}} \end{aligned} \quad (3)$$

The non-bond interaction term, E_{nonbond}, accounts for the interactions between non-bonded atoms and includes the van der Waals energy, E_{vdW}, the Coulomb electrostatic energy, E_{Coulomb}, and the hydrogen bond energy, E_{hbond}, as:

$$E_{\text{non-bond}} = E_{\text{vdW}} + E_{\text{Coulomb}} + E_{\text{hbond}} \quad (4)$$

Inter- and intra-molecular atomic interactions in the SWCNT + toluene system described in the previous section are modeled using COMPASS (Condensed-phased Optimized Molecular Potential for Atomistic Simulation Studies), the first *ab initio* forcefield that enables an accurate and simultaneous prediction of various gas-phase and condensed-phase properties of organic and inorganic materials [17–19]. The COMPASS forcefield uses the following expression for various components of the potential energy:

$$\begin{aligned} E_{\text{bond}} = {} & \sum_b \lfloor K_2(b-b_0)^2 + K_3(b-b_0)^3 \\ & + K_4(b-b_0)^4 \rfloor \end{aligned} \quad (5)$$

$$\begin{aligned} E_{\text{angle}} = {} & \sum_\theta \lfloor H_2(\theta-\theta_0)^2 + H_3(\theta-\theta_0)^3 \\ & + H_4(\theta-\theta_0)^4 \rfloor \end{aligned} \quad (6)$$

$$\begin{aligned} E_{\text{torsion}} = {} & \sum_\phi \Big\lfloor V_1 \big\lfloor 1 - \cos\left(\phi - \phi_1^0\right) \big\rfloor \\ & + V_2 \big\lfloor 1 - \cos\left(2\phi - \phi_2^0\right) \big\rfloor \\ & + V_3 \big\lfloor 1 - \cos\left(3\phi - \phi_3^0\right) \big\rfloor \Big\rfloor \end{aligned} \quad (7)$$

$$E_{\text{oop}} = \sum_x K_{\text{x}} \chi^2 \quad (8)$$

$$E_{\text{bond-bond}} = \sum_b \sum_{b'} F_{bb'}(b-b_0)(b'-b_0') \quad (9)$$

$$E_{\text{angle-angle}} = \sum_\theta \sum_{\theta'} F_{\theta\theta'}(\theta-\theta_0)(\theta'-\theta_0') \quad (10)$$

$$E_{\text{bond-angle}} = \sum_b \sum_\theta F_{b\theta}(b-b_0)(\theta-\theta_0) \quad (11)$$

$$\begin{aligned} E_{\text{end\_bond-torsion}} = {} & \sum_b \sum_\phi F_{b\phi}(b-b_0)[V_1 \cos\phi \\ & + V_2 \cos 2\phi + V_3 \cos 3\phi] \end{aligned} \quad (12)$$

$$\begin{aligned} E_{\text{middle\_bond-torsion}} = {} & \sum_{b'} \sum_\phi F_{b'\phi}(b'-b_0') \\ & \times [F_1 \cos\phi + F_2 \cos 2\phi + F_3 \cos 3\phi] \end{aligned} \quad (13)$$

$$\begin{aligned} E_{\text{angle-torsion}} = {} & \sum_\theta \sum_\phi F_{\theta\phi}(\theta-\theta_0)[V_1 \cos\phi \\ & + V_2 \cos 2\phi + V_3 \cos 3\phi] \end{aligned} \quad (14)$$

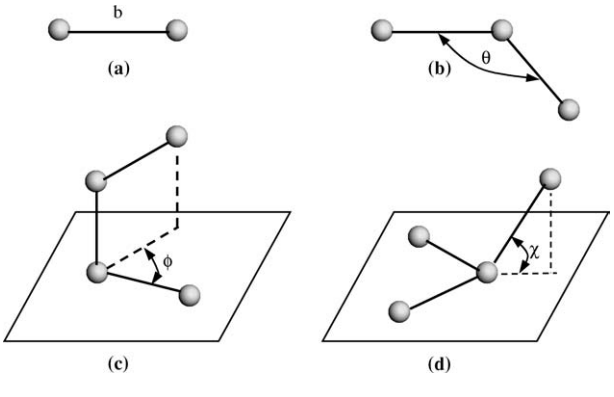

Figure 3 A schematic of the: (a) stretch, (b) angle, (c) torsion, and (d) inversion valence atomic interactions.

$$E_{\text{angle-angle-torsion}} = \sum_{\phi}\sum_{\theta}\sum_{\theta'} K_{\phi\theta\theta'} \times \cos\phi(\theta-\theta_0)(\theta'-\theta'_0) \quad (15)$$

$$E_{\text{Coulomb}} = \sum_{i>j} \frac{q_i q_j}{\varepsilon r_{ij}} \quad (16)$$

$$E_{\text{vdW}} = \sum_{i>j}\left[\frac{A_{ij}}{r_{ij}^9} - \frac{B_{ij}}{r_{ij}^6}\right] \quad (17)$$

where b and b' are the bond lengths, θ the two-bond angle, ϕ the dihedral torsion angle, χ the out of plane angle, q the atomic charge, ε the dielectric constant, r_{ij} the i-j atomic separation distance. b_0, $K_i(i = 2\text{–}4)$, θ_0, H_i $(i = 2\text{–}4)$, ϕ_i^0 $(i = 1\text{–}3)$, $V_i(i = 1\text{–}3)$, $F_{bb'}$, b'_0, $F_{\theta\theta'}$, θ'_0, $F_{b\theta}$, $F_{b\phi}$, $F_{b'\phi}$, $F_i(i = 1\text{–}3$, $F_{\theta\phi}$, $K_{\phi\theta\theta'}$, A_{ij}, and B_{ij} are the system dependent parameters implemented into Discover [20], the atomic simulation program used in the present work.

3. Results and discussion

3.1. Pure liquid toluene

To analyze the structure of the pure toluene (toluene in the absence of a SWCNT), a radial distribution function and several angular parameters plots are generated using the simulation results and analyzed in this section.

A number density radial distribution function for pure toluene is displayed in Fig. 4a. The radial positions indicated are associated with the center of mass of the toluene molecules. A simple observation of the results shown in Fig. 4a indicates the presence of a well-defined first solvation shell and a diffuse second solvation shell surrounding toluene molecules. The results obtained are very similar to the ones reported by Kim and Lee [21].

A probability density plot for the angle the bond between the methyl group and the benzene ring makes with the benzene-ring plane is shown in Fig. 5a. It is seen that while the most probable value of this angle is zero deg. (the value in the geometrically optimized structure of an isolated toluene molecule), a substantial fraction of toluene molecules have this angle as large as 10 deg. This finding suggests that interactions between the toluene molecules cause minor distortions in the structure of toluene molecules.

A probability density plot for the angle the benzene-ring normal makes with one of the principal coordinates (arbitrarily chosen as the z-axis) is plotted in Fig. 5b. A dashed line is also shown in Fig. 5b which represents the corresponding radial distribution function ($f(\theta) = \pi/360\sin(\theta)$, where θ is in degrees) associated with a random distribution of toluene molecules. By comparing the simulation results with the dashed curve, it can be concluded that the structure of pure toluene, past the first solvation shell, is quite random.

A probability density plot for the angle the bond between the methyl group and the benzene ring makes with the z-axis is plotted in Fig. 5c. Again, the corresponding probability density function for a random distribution of toluene molecules is displayed. It is seen that with respect to this angular parameter, the structure of the pure toluene appears also quite random.

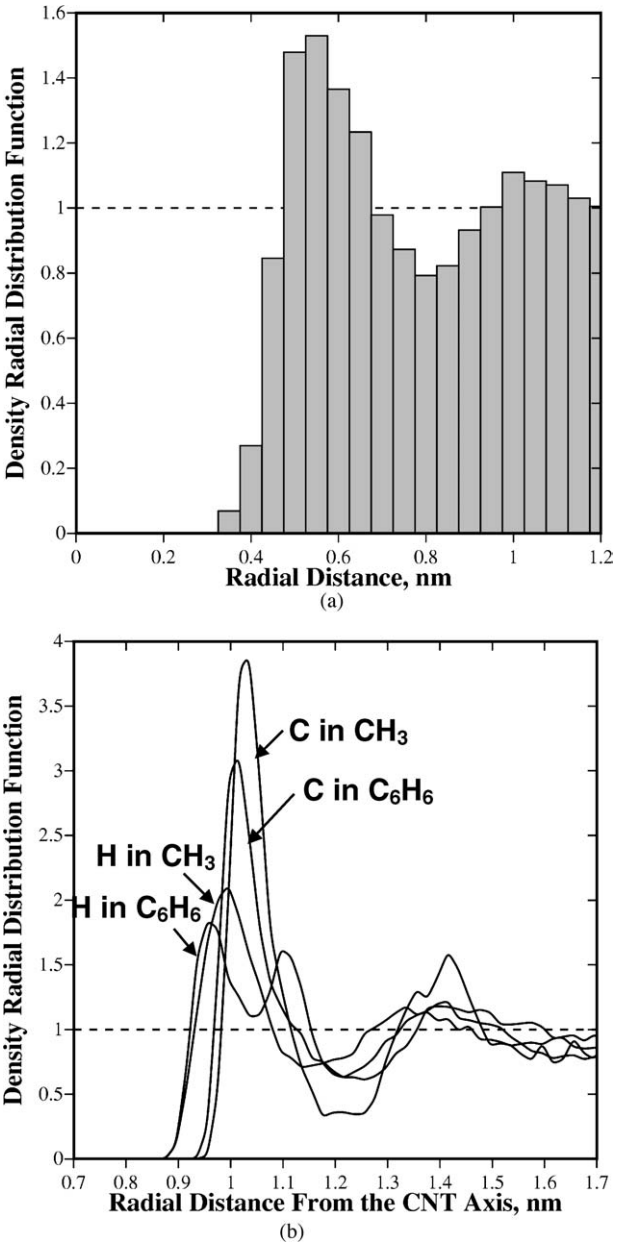

Figure 4 Number-density radial distribution function for: (a) pure toluene and (b) toluene containing a SWCNT.

3.2. Single SWCNT solubilized in toluene

3.2.1. The structure of toluene in the presence of a SWCNT

The structure of toluene in the presence of a SWCNT is analyzed using the number-density radial distribution function for carbon and hydrogen atoms in the toluene, as well as by examining the orientation of the toluene molecules with respect to the axis of the nanotube. The effect of SWCNT on the structure of individual toluene molecules (primarily the orientation of the methyl/benzene-ring bond) is also studied.

The number-density radial distribution function results for toluene in the presence of a SWCNT is shown in Fig. 4b. Separate plots are generated for carbon and hydrogen in the benzene ring and the carbon and hydrogen in the methyl group. The results displayed in

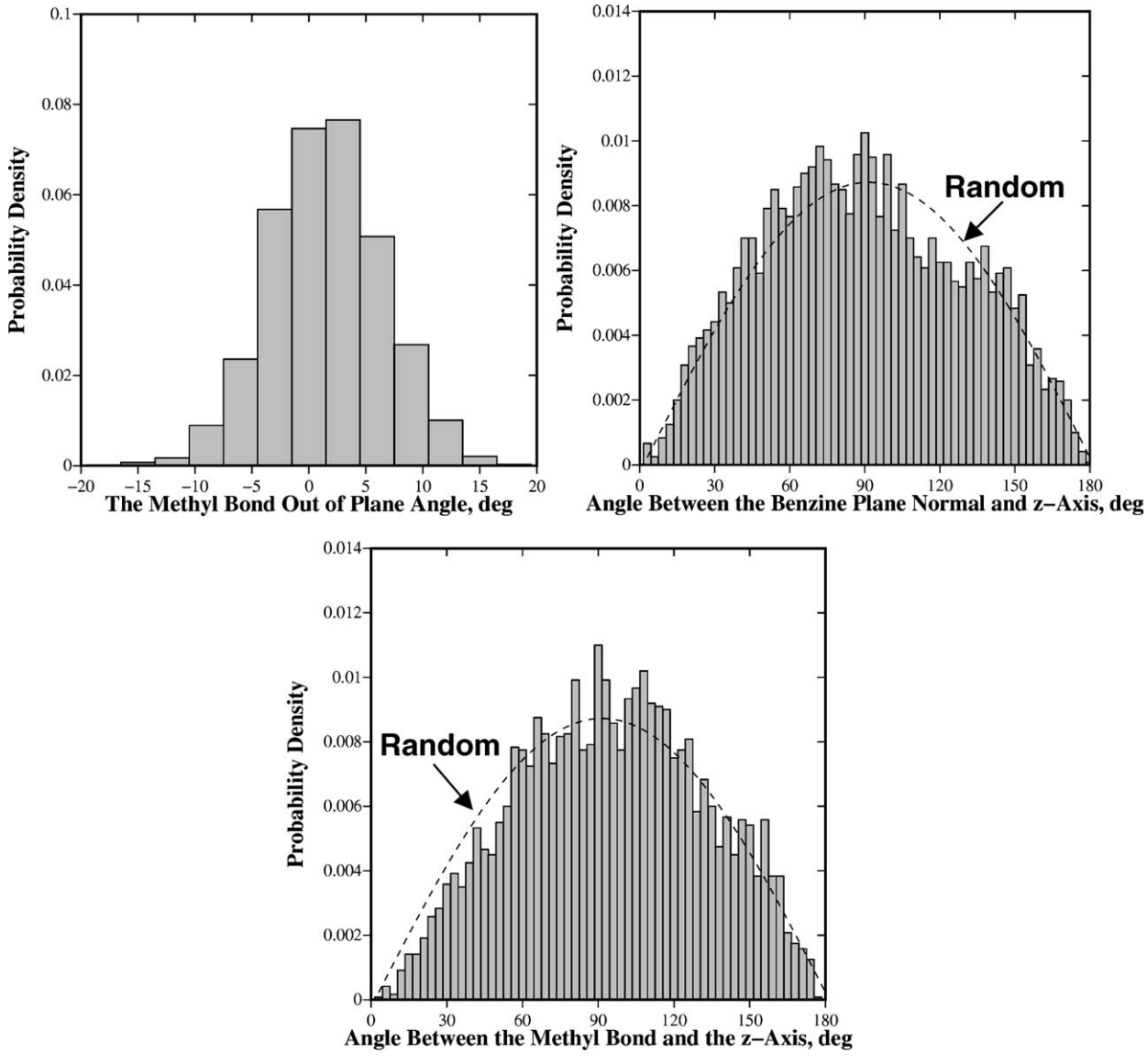

Figure 5 Angular parameters characterizing the structure of pure toluene. Please see text for details.

Fig. 4b can be summarized as follows:

(a) Toluene molecules surrounding the SWCNT form a well-defined first and a more-diffuse second solvation shell; and

(b) The orientation of toluene molecules in the first solvation shell is such that the benzene-ring portion of these molecules is closer to the nanotube axis then the methyl-group part of these molecules. A more complete picture about the orientation of toluene molecules is obtained using the analysis presented below.

A probability density plot for the angle, the methyl bond makes with the benzene plane for toluene molecules in the first solvation shell is displayed in Fig. 6a. By comparing the results displayed in Figs 6a and 5a, it can be concluded that the presence of SWCNT does not significantly affect the toluene intra-molecular angle in question, and hence, most likely does not significantly affect the structure of toluene molecules relative to that in the pure solvent.

A probability density plot for the angle between the benzene plane normal of the toluene molecules in the first solvation shell and the carbon nanotube axis is displayed in Fig. 6b. The results displayed suggest that the toluene molecules in the first solvation shell tend to align themselves in such a way that their benzene plane is parallel to the SWCNT axis. When an analogous plot was generated for the second solvation shell (the results not shown for the brevity), no significant reorientation of the toluene molecules relative to the structure of pure toluene is observed.

A probability density plot for the angle, the bond between the methyl group and the benzene ring makes with the SWCNT axis, for the toluene molecules in the first solvation shell is displayed in Fig. 6c. It is seen that the most probable values for this angle are ∼30 deg. and 120 deg. This finding suggests that one of the carbon-carbon bonds in the benzene ring involving the carbon atom of the benzene ring which is bonded to the methyl group, is nearly orthogonal to the SWCNT axis.

A probability density plot for the angle between radial vectors connecting the SWCNT axis and the center of the benzene ring and the benzene ring normal, for the toluene molecules in the first solvation shell, is

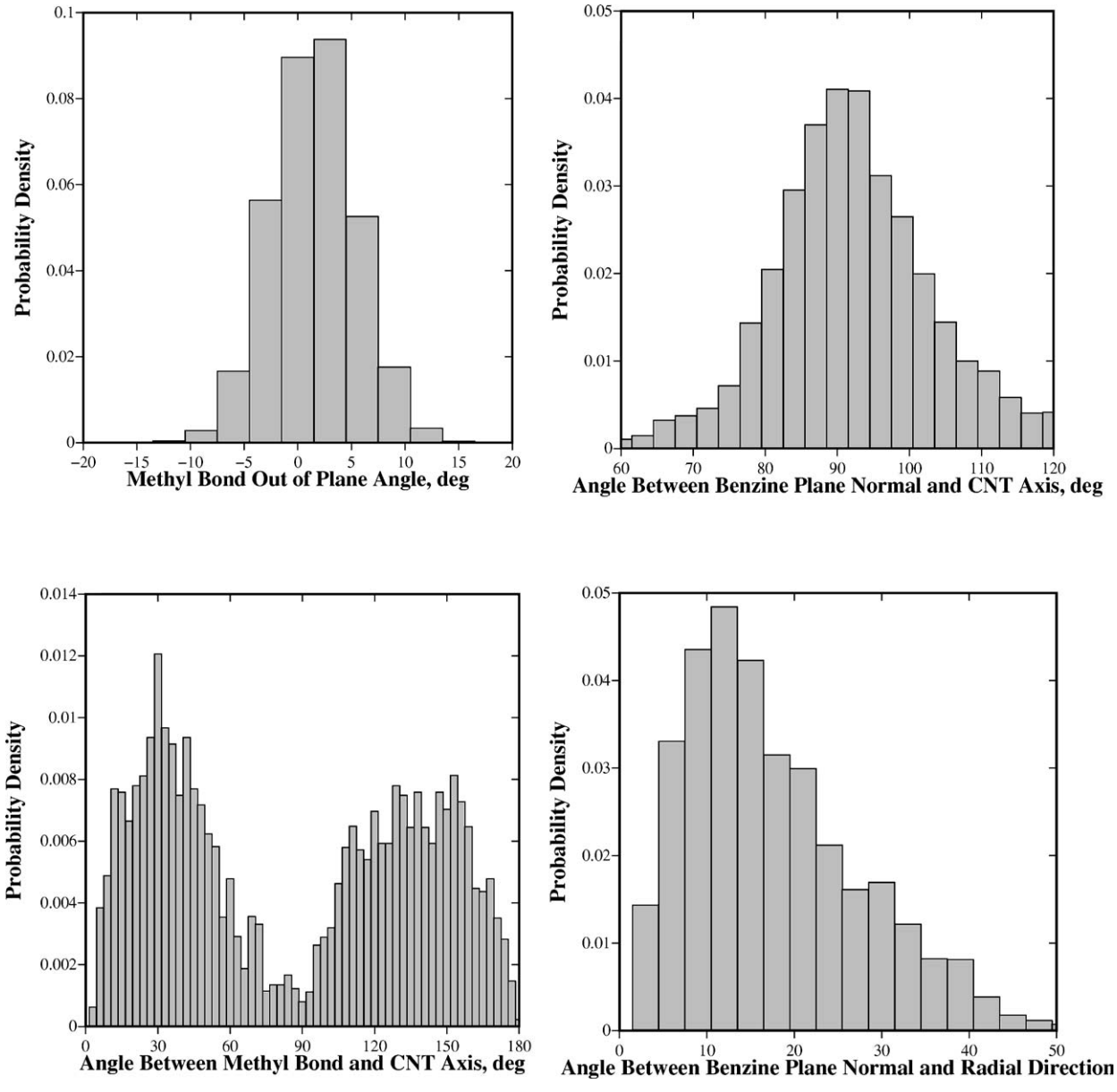

Figure 6 Angular parameter characterizing the structure of toluene in the presence of a SWCNT. Please see text for details.

displayed in Fig. 6d. The results displayed in this figure combined with the ones shown in Fig. 6b suggest that the benzene plane of the toluene molecules in the first solvation shell is tangential to the cylindrical walls of the first solvation shell.

3.2.2. SWCNT solvation energy in toluene

Molecular dynamic simulation results averaged over the last 5 ps of the simulation time are also used to analyze the energetics of the process of the introduction of a SWCNT from the vacuum into the bulk toluene solvent. The total energy change accompanying this process, $\Delta E_{\mathrm{T+SWCNT}}$, generally referred to as the *solvation energy*, has three contributions, i.e.:

$$\Delta E_{\mathrm{T+SWCNT}} = \Delta E_{\mathrm{T}} + \Delta E_{\mathrm{SWCNT}} + E^{\mathrm{Int}}_{\mathrm{T+CNT}} \quad (18)$$

where, ΔE_{T} represents a change in the solvent (toluene) energy accompanying the creation of a cylindrical cavity needed to accommodate the SWCNT. ΔE_{T} (analyzed below in more details) has two contributions itself, one associated with a change in the bulk structure of the solvent caused by the presence of the solute (SWCNT) and the other associated with the surface energy of the cylindrical cavity. $\Delta E_{\mathrm{SWCNT}}$ in Equation 18 represents a change in the SWCNT energy due to solvent/solute interactions. $\Delta E_{\mathrm{SWCNT}}$ is primarily the result of the changes in the carbon-carbon inter-atomic distances within the SWCNT caused by interactions between the SWCNT and the toluene molecules in the first solvation shell. $E^{\mathrm{Int}}_{\mathrm{SWCNT}}$ is the energy of the interaction between the atoms/molecules of the solvent and the solute.

Based on the atomic-scale simulations results obtained, the following energy change accompanying introduction of a SWCNT in toluene is obtained:

$$\begin{aligned}\Delta E_{\mathrm{T+SWCNT}} &= E_{\mathrm{T+SWCNT}} - E^{\circ}_{\mathrm{T}} - E^{\circ}_{\mathrm{SWCNT}} \\ &= 128{,}805.0 - (-14{,}472.8) \\ &\quad - 145{,}592.7 = -2{,}314.9\ \mathrm{kJ/mol}\end{aligned}$$

where E_T° and E_{SWCNT}° are the molar energies of the bulk toluene and the pristine SWCNT in the vacuum, respectively. Superscript zero is used in the remainder of the paper to denote various quantities of the pure substances in vacuum. It should be noted that the term *mole* used in the present paper pertains to the Avogadro's number of computational cells. In order words, all species within a computational cell are treated as one (complex) molecule.

The average changes in the molar energies of the bulk toluene and the SWCNT are found as follows:

$$\begin{aligned}\Delta E_T &= E_T - E_T^\circ = -14{,}078.2 - (-14{,}472.8)\\ &= 394.6 \text{ kJ/mol}, \quad \text{and}\\ \Delta E_{SWCNT} &= E_{SWCNT} - E_{SWCNT}^\circ\\ &= 145{,}596.9 - 145{,}992.7 = 4.2 \text{ kJ/mol}.\end{aligned}$$

The interaction energy between the toluene and the SWCNT, E_{SWCNT}^{Int}, is computed as:

$$\begin{aligned}E_{T+SWCNT}^{Int} &= \Delta E_{T+SWCNT} - \Delta E_T - \Delta E_{SWCNT}\\ &= -2{,}314.9 - 394.6 - 4.2\\ &= -2{,}713.7 \text{ kJ/mol}\end{aligned}$$

Since the total energy change associated with the introduction of a SWCNT into the toluene ($\Delta E_{T+SWCNT} = -2,314.9$ kJ/mol) is negative, our preliminary finding is that the SWCNTs should be soluble in this solvent. However, to obtain a definite answer to this question, one must also consider the entropy change accompanying the introduction of a SWCNT into the toluene. An analysis of the SWCNT solvation entropy in toluene is next section.

The results presented above show that the change in the toluene energy due to introduction of a SWCNT, $\Delta E_T = 394.6$ kJ/mol, makes a significant contributions to the SWCNT solvation energy. As mentioned above, this component of the solvation energy arises from the creation of a surface in the cylindrical cavity and due to the rearrangement of toluene molecules (primarily the ones in the first and the second solvation shells surrounding the SWCNT). To assess the relative magnitudes of the two contributions to ΔE_T, the surface energy of toluene is first computed by carrying out molecular dynamics simulations described earlier but for a slab (instead for a bulk) geometry of the toluene computational cell. The slab is obtained by removing the periodic boundary conditions in one of the principal directions of the bulk computational cell which results in the formation of two parallel surfaces per computational cell. The surface energy of toluene is next obtained as:

$$\begin{aligned}E_T^{surf,flat} &= \frac{\left(E_T^{\circ,slab} - E_T^\circ\right)}{N_A A}\\ &= \frac{-4335.1 \times 10^3 + 4468.4 \times 10^3}{N_A \times 2 \times (26.04 \times 10^{-10})^2}\\ &= 0.016 \text{ J/m}^2\end{aligned}$$

where the energies are expressed in J/mol. N_A is the Avogadro's number and A the exposed surface area in m^2. The value of the surface energy (0.016 J/m^2) is not in very good agreement with its experiment counterpart, 0.018 J/m^2 [22].

Since the cavity that accommodates a SWCNT within the solvent is cylindrical, the curvature of its surface can, in principle, have an effect on the surface energy. To quantify this effect, attempts were made to carry out geometrical optimization of the toluene structure containing a cylindrical cavity. Unfortunately, the attempts were not successful since the cavity was unstable and was quickly filled by the surrounding toluene molecules. Consequently, a different strategy was pursued. The effect of the surface curvature on the surface energy was assessed by comparing the surface energies of unrelaxed (geometrically un-optimized) structures of the slab toluene and the one containing a cylindrical cavity. The average (unrelaxed) surface energy of a flat toluene surface is calculated as:

$$\begin{aligned}E_T^{surf,flat,unrel} &= \frac{\left(E_T^{\circ,slab}, \text{unrel} - E_T^\circ\right)}{N_A A}\\ &= \frac{757.4 \times 10^3 - 88.8 \times 10^3}{N_A \times 2 \times (26.04 \times 10^{-10})^2}\\ &= 0.082 \text{ J/ m}^2\end{aligned}$$

while the corresponding surface energy of the cylindrical cavity is computed as:

$$\begin{aligned}E_T^{surf,cyl,unrel} &= \frac{\left(E_T^{\circ,cyl} - E_T^\circ\right)}{N_A A}\\ &= \frac{4330.9 \times 10^3 - 3612.8 \times 10^3}{N_A \times 2\pi \times 9.9 \times 26.04 \times 10^{-20}}\\ &= 0.074 \text{ J/m}^2\end{aligned}$$

The two surface energy values, which differ by about around 10%, suggest that the curvature most likely does not affect the surface energy (in the relaxed structures) very significantly.

The energy change of the toluene arising from formation of a cylindrical cavity which accommodates the SWCNT is next calculate by multiplying the calculated surface energy with the surface area of the cylindrical cavity as:

$$\begin{aligned}E_T^{surf,cyl} &= 0.016 \times N_A \times (2\pi \times 9.9 \times 26.049\\ &\quad \times 10^{-20}) \times 10^{-3} = 254.1 \text{ kJ/mol}\end{aligned}$$

A comparison of this value with $\Delta E_T = 394.6$ kJ/mol suggests that the energy change of the toluene associated with formation of a cylindrical cavity represents almost two thirds of the total energy change of the toluene asoociated with the introduction of a SWCNT.

3.2.3. SWCNT solvation entropy in toluene

The molar entropy of pure toluene can be expressed as a sum of the corresponding ideal-gas molar entropy, S_T^{ig}, and the molar excess entropy, S_T^{ex}, as:

$$S_T = S_T^{ig} + S_T^{ex} \tag{19}$$

where all three quantities in Equation 19 are evaluated at a given volume, V, and temperature, T, conditions of the system.

The ideal-gas molar entropy can be expressed as:

$$S_T^{ig} = \frac{5R_u}{2} - R_u \ln\left(\rho_T \Lambda_T^3\right) \tag{20}$$

where R_u is the universal gas constant, ρ_T the number density of toluene and Λ_T the corresponding thermal de Broglie wavelength defined as:

$$\Lambda_T = \left(\frac{h^2}{2\pi m_T k_B T}\right)^{\frac{1}{2}} \tag{21}$$

where h is the Planck's constant, m_T is the molecular mass of toluene, and k_B the Boltzmann's constant.

The molar excess entropy can be defined as a sum of two-, three-, and higher order many-body contributions. Computational studies of liquid metals [23], noble gases [24], hard-sphere fluids [24, 25], and Lennard-Jones fluids [25, 26] at liquid-like densities, showed that the molar excess entropy is dominated, and hence can be reasonably well approximated, by the two-body term. This simplification is utilized in the present work.

If the toluene molecules are considered tentatively as spherically shaped for simplicity, the toluene two-body (pair) correlation function depends only on the relative position vector, r, of the molecules. Under such approximation, the molar excess entropy of toluene can be expressed as:

$$S_T^{ex} = -\frac{R_u \rho_T^2}{2} \int g(r) \ln(g(r))\, dv + \frac{R_u \rho_T^2}{2} \int [g(r) - 1]\, dv \tag{22}$$

where $g(r)$ is the pair correlation function and the integration is carried out over the system volume.

Under a similar assumption, the molar entropy of a solution consisting of SWCNTs suspended in toluene can be expressed as:

$$\begin{aligned} S_{T+SWCNT} &= \frac{5R_u(1 - x_{SWCNT})}{2} - R_u(1 - x_{SWCNT}) \ln\left(\rho_T \Lambda_T^3\right) \\ &+ \frac{5R_u x_{SWCNT}}{2} - R_u x_{SWCNT} \ln\left(\rho_{SWCNT} \Lambda_{SWCNT}^3\right) \\ &- \frac{R_u(1 - x_{SWCNT})\rho_T}{2} \\ &\times \left\{ \int g_{T,T}(r) \ln[g_{T,T}(r)]\, dv - \int [g_{T,T}(r) - 1]\, dv \right\} \\ &- R_u x_{SWCNT} \rho_T \left\{ \int g_{SWCNT,T}(r) \ln[g_{SWCNT,T}(r)]\, dv \right. \\ &\left. - \int [g_{SWCNT,T}(r) - 1]\, dv \right\} - \frac{R_u x_{SWCNT} \rho_{SWCNT}}{2} \\ &\times \left\{ \int g_{SWCNT,SWCNT}(r) \ln[g_{SWCNT,SWCNT}(r)]\, dv \right. \\ &\left. \times \int [g_{SWCNT,SWCNT}(r) - 1]\, dv \right\} \end{aligned} \tag{23}$$

where x_{SWCNT} is the mole fraction of SWCNTs in the solution, and $g_{T,T}$, $g_{T,SWCNT}$, and $g_{SWCNT,SWCNT}$ are the toluene-toluene, toluene-SWCNT and SWCNT-SWCNT pair correlation functions, respectively.

The partial molar entropy of the solute, $\bar{S}_{SWCNT}$, is obtained by differentiating Equation 23 with respect to $N_{SWCNT} = N_{AV} x_{SWCNT}$ under constant T, V and $N_T = N_{AV}(1 - x_{SWCNT})$ where N_{AV} is the Avogadro's number. In the limit of infinite dilution, this procedure yields:

$$\begin{aligned} \bar{S}_{SWCNT} &= \frac{3R_u}{2} - R_u \ln\left(\rho_{SWCNT} \Lambda_{SWCNT}^3\right) \\ &- R_u \rho_T \left[\int g_{SWCNT,T} \ln g_{SWCNT,T}\, dv \right. \\ &\left. \times - \int (g_{SWCNT,T} - 1)\, dv \right] - \frac{R_u \rho_T^2}{2} \\ &\times \int \left(\frac{\partial g_{T,T}}{\partial \rho_{SWCNT}} \right)_{T,V,N_T}^{\infty} \ln(g_{T,T})\, dv \end{aligned} \tag{24}$$

The first two terms in Equation 24, reflect the ideal-gas contributions, while the last two terms are associated with the solute-solvent correlation function. Following Ashbaugh and Paulaitis [27], the last term in Equation 24 can be neglected since it generally makes a small contribution to the solvation entropy.

Also, following the procedure described by Ashbaugh and Paulaitis [27], the standard solvation entropy $\Delta S_{T+SWCNT}$ is related to the partial molar entropy of solute, $\bar{S}_{SWCNT}$, as:

$$\begin{aligned} \Delta S_{T+SWCNT} &= \bar{S}_{SWCNT} - R_u \ln\left(\rho_{SWCNT} \Lambda_{SWCNT}^3\right) \\ &- R_u T \alpha_T - \frac{3R_u}{2} \end{aligned} \tag{25}$$

where $\alpha_T = 9.6 \times 10^{-6}$/K is the thermal expansion coefficient of toluene. Substitution of Equation 24 into Equation 25 yields:

$$\begin{aligned} \Delta S_{T+SWCNT} &= -R_u T \alpha_T - R_u \rho_{\mathbf{T}} \left[\int g_{SWCNT,T} \ln g_{SWCNT,T}\, dv \right. \\ &\left. - \int (g_{SWCNT,T} - 1)\, dv \right] \end{aligned} \tag{26}$$

The second term in the Equation 26, is generally referred to as *the solute-solvent correlation entropy* and

under the assumption of spherical shapes of the solvent and solute molecules, the pair correlation function depends only on the radial distance, r. However, in the present case where toluene molecules are plate-like and the SWCNT has a cylindrical shape, the pair-correlation function involves additional degrees of freedom which are required to describe solute-solvent orientations and conformations. In the present work, it is assumed that within the first solvation shell of the SWCNT, the solute-solvent pair correlation function can be factorized into a radial part and an orientation-dependent part. Beyond the first solvation shell, on the other hand, the pair correlation function is assumed to involve only the radial part. Thus, the toluene-SWCNT pair correlation function is defined as:

$$g_{\mathrm{T,SWCNT}}(r,\alpha,\beta,\gamma) = \begin{cases} g^{\mathrm{rad}}_{\mathrm{T,SWCNT}}(r)\, g^{\mathrm{ang}}_{\mathrm{T,SWCNT}}(\alpha,\beta,\gamma) & r \le r_{\mathrm{sh}} \\ g^{\mathrm{rad}}_{\mathrm{T,SWCNT}}(r) & r > r_{\mathrm{sh}} \end{cases} \quad (27)$$

where α, β and γ are Euler angles (defined below), r_{sh} the radius of the first solvation shell, while superscripts *rad* and *ang* are used to denote the radial and the angular (orientation-dependent) components of the pair correlation function. For the toluene-SWCNT pair correlation function given by Equation 27, the solvation entropy originally defined by Equation 26 becomes:

$$\begin{aligned} \Delta S_{\mathrm{T+SWCNT}} &= -R_{\mathrm{u}} T \alpha_{\mathrm{T}} - R_{\mathrm{u}} \rho_{\mathrm{T}} \left\{ \int_V g^{\mathrm{rad}}_{\mathrm{T,SWCNT}}(r) \right. \\ &\quad \left. \times \ln\left[g^{\mathrm{rad}}_{\mathrm{T,SWCNT}}(r) \right] \mathrm{d}v - \int_V \left[g^{\mathrm{rad}}_{\mathrm{T,SWCNT}}(r) - 1 \right] \mathrm{d}v \right\} \\ &\quad - \frac{R_{\mathrm{u}} \rho_{\mathrm{T}}}{A_{\mathrm{Norm}}} \left\{ V_{\mathrm{sh}} \iiint g^{\mathrm{ang}}_{\mathrm{T,SWCNT}}(\alpha,\beta,\gamma) \right. \\ &\quad \left. \times \ln\left[g^{\mathrm{ang}}_{\mathrm{T,SWCNT}}(\alpha,\beta,\gamma) \right] \sin\beta \; \mathrm{d}\alpha \times \mathrm{d}\beta \times \mathrm{d}\gamma \right\} \end{aligned} \quad (28)$$

where A_{Norm} is the normalization factor for the angular part of the pair-correlation function (defined below) and the V_{sh} term represents the integral of the radial part of the pair distribution function over the volume of the first solvation shell.

The orientation of each toluene molecule with respect to the nanotube axis is defined using three Euler angles. Before quantifying Euler angles for each toluene molecule, a Cartesian coordinate system is attached to such a molecule as shown in Fig. 7. The x- and z-axes of the coordinate system are aligned with the methyl-bond direction, R_{m}, and the benzene-plane normal, R_{n}, respectively. The y-axis in the same coordinate system is then obtained as $y = R_{\mathrm{n}} \times R_{\mathrm{m}}$, where $\times$ is used to denote a cross product of two vectors. It should be noted that since toluene molecules are distorted, as shown in Section 3.2.1, a simple procedure was developed to determine the "effective" benzene-plane normal and the "effective" methyl-bond direction

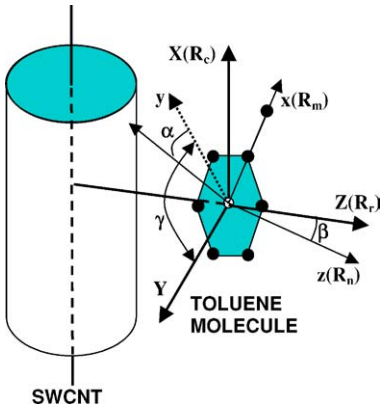

Figure 7 The SWCNT-based X-Y-Z and the toluene molecule-based x-y-z Cartesian coordinate systems used in the present work.

for toluene molecules before the coordinate system described above can be constructed. Next, a Cartesian coordinate system associated with the SWCNT is next constructed in the following way: the X-axis is aligned with the SWCNT axis, while the Z-axis is aligned with a radial direction originating from the SWCNT axis and passing through the center of the benzene plane of the toluene molecule in question. The Y-axis is then defined as $Y = Z \times X$. Once the two coordinate systems are established, the three Euler angles are defined as following: α is defined as the angle between $z \times Z$ and y, β as the angle between z and Z and γ as the angle between $z \times Z$ and Y. The ranges of the three Euler angles are $0 \le \alpha < 2\pi$, $0 \le \beta \le \pi$ and $0 \le \gamma < 2\pi$. Since a differential element of the solid angle is defined as: $\mathrm{d}\Omega = \sin\beta \cdot \mathrm{d}\alpha \cdot \mathrm{d}\beta \cdot \mathrm{d}\gamma$, and the integration of $\mathrm{d}\Omega$ between the limits of α, β and γ stated above yields $A_{\mathrm{Norm}} = 8\pi^2$, A_{Norm} is the appropriate normalization factor in the angular part of the pair-correlation function.

The solvation entropy for SWCNTs in toluene is then calculated using Equation 28 and the atomistic simulation results for the last 5 ps of the simulation time. Integrals appearing in Equation 28 are evaluated numerically using the trapezoid rule. Due to the cylindrical geometry of the SWCNT, the volume element appear in Equation 28 is defined as $\mathrm{d}v = 2\pi a_z r \mathrm{d}r$, where a_z is the computational-cell lattice parameter in z-direction. The radial and the angular components of the toluene-SWCNT pair-correlation function are evaluated numerically by constructing the corresponding frequency functions. The results of this procedure yielded the solvation entropy for SWCNT in toluene of $\Delta S_{\mathrm{T+SWCNT}} = -8.6$ kJ/mol/K. Using this value of solvation entropy, the solvation Gibbs free energy is evaluated as:

$$\begin{aligned} \Delta G_{\mathrm{T+SWCNT}} &= \Delta E_{\mathrm{T+SWCNT}} - T \Delta S_{\mathrm{T+SWCNT}} \\ &= -2042.0 - 298.0 \times (-8.6) \\ &= 495 \text{ kJ/mol} \end{aligned}$$

where one mole is defined as the Avogadro's number of computational cells. Since this value of the solvation Gibbs free energy is small (one computational cell contains 330 toluene molecules) but positive, one would

expect that SWCNTs could be relatively easily suspend in toluene but the resulting suspension would not be stable and, given enough time, SWCNTs would drop out of solution. This prediction is fully consistent with the experimental observation made by in het Panhuis *et al.* [28] during their attempts to solubilize SWCNTs in toluene.

4. Conclusions

Based on the results obtained in the present work, the following main conclusions can be drawn:

1. Introduction of the SWCNTs into toluene is associated with a relatively small but negative solvation energy. The largest contribution to be solvation energy arises from the SWCNT-toluene interactions.

2. Interactions between SWCNTs and toluene molecules result in major reorganization of the toluene molecules and the associated conformation gives rise to a substantial decrease in the configurational entropy of the toluene.

3. The solvation Gibbs free energy of SWCNTs in toluene at room temperature is relatively small but positive suggesting that suspension of SWCNTs in toluene is not stable. This prediction is consistent with experimental observations.

Acknowledgements

The material presented in this paper is based on work supported by the U.S. Army Grant Number DAAD19-01-1-0661. The authors are indebted to Drs. Bonnie Gersten, Fred Stanton and William DeRosset of ARL for the support and a continuing interest in the present work.

References

1. S. IIJIMA, *Nature* **354** (1991) 56.
2. M. GRUJICIC, G. CAO and B. GERSTEN, *Appl. Surf. Sci.* **206** (2003) 167.
3. S. J. TANS, R. M. VERSCHUEREN and C. DEKKER, *Nature* **393** (1999) 40.
4. A. C. DILLON, K. M. JONES, T. A. BEKKEDAHL, C. H. KIANG, D. S. BETHUNE and M. J. HEBEN, *ibid.* **386** (1997) 377.
5. M. M. J. TREACY, T. W. EBBESEN and J. M. GIBSON, *ibid.* **381** (1996) 678.
6. P. G. COLLINS, K. BRADLEY, M. ISHIGSMI and A. ZETTL, *Science* **287** (2000) 1801.
7. J. N. COLEMAN, A. B. DALTON, S. CURRAN, A. RUBIO, A. P. DAVEY, A. DRURY, B. McCARTHY, B. LAHR, P. M. AJAYAN, S. ROTH, R. C. BARKLIE and W. J. BLAU, *Adv. Mater.* **12** (2000) 213.
8. M. IN HET PANHUIS, A. MAITI, A. B. DALTON, A. V. D. NOORT, J. N. COLEMAN, B. McCARTHY and W. J. BLAU, *J. Phys. Chem.* B **107** (2003) 478.
9. B. McCARTHY, J. N. COLEMAN, R. CZERW, A. B. DALTON, M. IN HET PANHUIS, A. MAITI, A. DRURY, H. J. BYRNE, D. L. CARROLL and W. J. BLAU, *ibid.* **106** (2002) 2210.
10. A. DRURY, S. MAIER, A. P. DAVEY, A. B. DALTON, J. N. COLEMAN, H. J. BYRNE and W. J. BLAU, *J. Synth. Met.* **119** (2001) 151.
11. S. CURRAN, P. AJAYAN, W. BLAU, D. CARROLL, J. COLEMAN, A. DALTON, A. P. DAVEY, B. McCARTHY and A. STREVENS, *Adv. Mater.* **10** (1998) 1091.
12. S. CURRAN, A. P. DAVEY, J. COLEMAN, A. DALTON, B. McCARTHY, S. MAIER, D. GRAY, M. BRENNAN, K. RYDER, M. L. DE LA CHAPELLE, C. JOURNET, P. BERNIER, H. J. BYRNE, D. CARROLL, P. M. AJAYAN, S. LEFRANT and W. J. BLAU, *Synthetic Met.* **103** (1999) 2559.
13. J. COLEMAN, A. DALTON, S. CURRAN, A. RUBIO, A. DAVEY, A. DRURY, B. McCARTHY, B. LAHR, P. AJAYAN, S. ROTH, R. BARKLIE and W. BLAU, *Adv. Mater.* **12** (2000) 213.
14. A. B. DALTON, C. STEPHAN, J. N. COLEMAN, B. McCARTHY, P. M. AJAYAN, S. LEFRANT, P. BERNIER, W. J. BLAU and H. J. BYRNE, *J. Phys. Chem.* B. **104**(43) (2000) 10012.
15. A. B. DALTON, W. J. BLAU, G. CHAMBERS, J. N. COLEMAN, K. HENDERSON, S. LEFRANT, B. McCARTHY, C. STEPHAN and H. J. BYRNE, *Synth. Met.* **121**(1–3) (2001) 1217.
16. B. McCARTHY, J. N. COLEMAN, S. A. CURRAN, A. B. DALTON, A. P. DAVEY, Z. KONYA, A. FONSECA, J. B. NAGY and W. J. BLAU, *J. Mater. Sci. Letts.* **19**(24) (2000) 2239.
17. H. SUN, *J. Phys. Chem.* B. **102** (1998) 7338.
18. H. SUN; P. REN and J. R. FRIED, *Comput. Theor. Polym. Sci.* **8**(1/2) (1998) 229.
19. D. RIGBY, H. SUN and B. E. EICHINGER, *Polym. Int.* **44** (1998) 311.
20. http://www.accelrys.com/mstudio/ms_modeling/discover.html
21. J. H. KIM and S. H. LEE, *Bull. Korean Chem. Soc.* **23** (2002) 441.
22. http://www.vp-scientific.com/hydrophobic_coating.htm
23. D. WALLACE, *J. Chem. Phys.* **87** (1987) 2282.
24. R. MOUNTAIN and H. RAVECHE, *ibid.* **53** (1971) 2250.
25. B. LAIRD and A. HAYMET, *Phys. Rev*. A **45** (1992) 5680.
26. K. I. BORZSA and A. BARANYAI, *Chem. Phys*. **165** (1992) 227.
27. H. S. ASHBAUGH and M. E. PAULAITIS, *J. Phys. Chem.* **100** (1996) 1900.
28. M. IN HET PANHUIS, A. MAITI, A. B. DALTON, A. V. D. NOORT, J. N. COLEMAN, B. McCARTHY and W. J. BLAU, *J. Phys. Chem.* B **107** (2003) 478.

Received 21 July
and accepted 6 October 2003